### 九州大学学術情報リポジトリ Kyushu University Institutional Repository

# The XP07-NPAT axis represents key vulnerabilities in TP53-mutated acute myeloid leukemia

#### Semba, Yuichiro

Department of Medicine and Biosystemic Science, Kyushu University Graduate School of Medical Sciences

#### Yamauchi, Takuji

Department of Medicine and Biosystemic Science, Kyushu University Graduate School of Medical Sciences

#### Bauer, Daniel E.

Boston Children's Hospital, Boston, Massachusetts

# Ogawa, Seishi

Kyoto University

他

https://hdl.handle.net/2324/7392676

出版情報: Blood Journal, 2025-10-29. American Society of Hematology

バージョン:

権利関係: Copyright © 2025 American Society of Hematology



Check for updates



American Society of Hematology 2021 L Street NW, Suite 900, Washington, DC 20036 Phone: 202-776-0544 | Fax 202-776-0545

# The XPO7-NPAT axis represents key vulnerabilities in TP53-mutated acute myeloid leukemia

Tracking no: BLD-2025-028918R2

Yuichiro Semba (Department of Medicine and Biosystemic Science, Kyushu University Graduate School of Medical Sciences, Japan) Takuji Yamauchi (Department of Medicine and Biosystemic Science, Kyushu University Graduate School of Medical Sciences, Japan) Daniel Bauer (Boston Children's Hospital, United States) Seishi Ogawa (Kyoto University, Japan) Koichi Akashi (Kyushu University Graduate School of Medical Sciences, Japan) Takahiro Maeda (Kyushu University Graduate School of Medical Sciences, Japan)

#### Abstract:

Acute myeloid leukemia (AML) with TP53 mutations is almost universally refractory to chemotherapy, molecular-targeted therapies, and hematopoietic stem cell transplantation, leading to dismal clinical outcomes. The lack of effective treatments underscores the urgent need for novel therapeutic strategies. Using genome-wide CRISPR/Cas9 dropout screens in isogenic Trp53-wild-type (WT) and knockout (KO) mouse AML models, combined with transcriptomic and proteomic analyses of mouse and human AML samples, we identify the XPO7 (exportin 7)-NPAT (nuclear protein, coactivator of histone transcription) pathway as essential for TP53-mutated AML cell survival. In TP53-WT AML, XPO7 functions as a tumor suppressor by regulating nuclear abundance of p53 protein, particularly when basal levels of functional p53 are high. However, in TP53-mutated AML, XPO7 drives leukemia proliferation by retaining NPAT, an XPO7-associated protein predominantly expressed in TP53-mutated AML, within the nucleus. NPAT depletion induces genome-wide histone loss, compromises genomic integrity, and triggers replication catastrophe in TP53-mutated AML cells. Notably, analysis of publicly available AML datasets, primary AML samples, and single-cell intra-patient mRNA profiles further reveals elevated XPO7 and NPAT expression in TP53-mutated AML. Finally, we validate the XPO7-NPAT pathway as a critical driver of leukemia progression in vivo using patient-derived xenograft (PDX) models of TP53-WT and TP53-mutant AML. Our study delineates key molecular mechanisms underlying TP53-mutated AML pathogenesis and identifies the XPO7-NPAT axis as a critical vulnerability in this refractory leukemia subtype.

Conflict of interest: No COI declared

COI notes:

Preprint server: No;

Author contributions and disclosures: Conceptualization, T.M.; methodology, Y.S., T.Y., D.B. and S.O.; Investigation, Y.S. and T.Y.; writing-original draft, Y.S. and T.M.; writing-review & editing, T.M.; funding acquisition, Y.S., T.Y., S.O., K.A. and T.M.; resources, K.A. and T.M.; supervision, S.O., K.A. and T.M.

Non-author contributions and disclosures: No;

Agreement to Share Publication-Related Data and Data Sharing Statement: emails to the corresponding author

Clinical trial registration information (if any):

# The XPO7-NPAT axis represents key vulnerabilities in *TP53*-mutated acute myeloid leukemia

3

1

2

4 Yuichiro Semba<sup>1,2</sup>, Takuji Yamauchi<sup>2</sup>, Daniel E. Bauer<sup>3</sup>, Seishi Ogawa<sup>4</sup>, Koichi Akashi<sup>2</sup> and
5 Takahiro Maeda<sup>1</sup>\*

6

- <sup>1</sup>Division of Precision Medicine, Kyushu University Graduate School of Medical Sciences,
- <sup>2</sup>Department of Medicine and Biosystemic Science, Kyushu University Graduate School of
- 9 Medical Sciences, Fukuoka, Japan. <sup>3</sup>Division of Hematology/Oncology, Boston Children's
- Hospital, Department of Pediatric Oncology, Dana-Farber Cancer Institute, Harvard Stem Cell
- Institute, Department of Pediatrics, Harvard Medical School, Boston, Massachusetts 02115,
- 12 USA. <sup>4</sup>Department of Pathology and Tumor Biology, Graduate School of Medicine, Kyoto
- 13 University, Kyoto, Japan.

14 15

\*Correspondence to:

17

16

- Takahiro Maeda M.D., Ph.D.
- 19 Division of Precision Medicine
- 20 Kyushu University Graduate School of Medical Sciences
- 3-1-1 Maidashi, Higashi-ku, Fukuoka, Fukuoka 812-8582, Japan
- Phone: +81-92-642-6572
- 23 Fax: +81-92-642-6679
- Email: maeda.takahiro.294@m.kyushu-u.ac.jp

- Abstract: 224 words
- 27 Text: 4478 words
- Figure: 6
- 29 Reference: 48

30	Key Points:
31	1. TP53 mutation rewires the histone gene regulatory network via the XPO7-NPAT pathway,
32	creating a potential vulnerability in TP53-mutated AML cells.
33	2. NPAT depletion compromises genomic integrity, causing replication catastrophe, particularly
34	in p53-deficient cells.
35	
36	Running Title:
37	The Achilles' heel of <i>TP53</i> -mutated AML
38	
39	Data Sharing Statement:
40	RNA-seq, ATAC-seq and scRNA-seq data were deposited in the Gene Expression Omnibus
41	(GEO) database under accession number GSE264596. For further information or data requests,
42	please contact maeda.takahiro.294@m.kyushu-u.ac.jp.

#### **Abstract**

44

45

46

47

48

49

50

51

52

53

54

55

56

57

58

59

60

61

62

63

64

Acute myeloid leukemia (AML) with TP53 mutations is almost universally refractory to chemotherapy, molecular-targeted therapies, and hematopoietic stem cell transplantation, leading to dismal clinical outcomes. The lack of effective treatments underscores the urgent need for novel therapeutic strategies. Using genome-wide CRISPR/Cas9 dropout screens in isogenic Trp53-wild-type (WT) and knockout (KO) mouse AML models, combined with transcriptomic and proteomic analyses of mouse and human AML samples, we identify the XPO7 (exportin 7)-NPAT (nuclear protein, coactivator of histone transcription) pathway as essential for TP53mutated AML cell survival. In TP53-WT AML, XPO7 functions as a tumor suppressor by regulating nuclear abundance of p53 protein, particularly when basal levels of functional p53 are high. However, in TP53-mutated AML, XPO7 drives leukemia proliferation by retaining NPAT, an XPO7-associated protein predominantly expressed in TP53-mutated AML, within the nucleus. NPAT depletion induces genome-wide histone loss, compromises genomic integrity, and triggers replication catastrophe in TP53-mutated AML cells. Notably, analysis of publicly available AML datasets, primary AML samples, and single-cell intra-patient mRNA profiles further reveals elevated XPO7 and NPAT expression in TP53-mutated AML. Finally, we validate the XPO7-NPAT pathway as a critical driver of leukemia progression in vivo using patient-derived xenograft (PDX) models of TP53-WT and TP53-mutant AML. Our study delineates key molecular mechanisms underlying TP53-mutated AML pathogenesis and identifies the XPO7-NPAT axis as a critical vulnerability in this refractory leukemia subtype.

#### Introduction

*TP53* encodes the transcription factor p53, which is crucial for cellular responses to stress and orchestrates numerous biological processes, such as cell cycle regulation, apoptosis, maintenance of genome integrity, and cellular plasticity <sup>1,2</sup>. As the "guardian of the genome", *TP53*'s pivotal role in tumor suppression is underscored by its status as the most frequently mutated gene in human cancers <sup>3</sup>. The impact of these mutations is highly variable and depends on cellular and molecular contexts <sup>1,4</sup>. Studies in solid cancers have delineated diverse functional consequences of *TP53* mutations, ranging from loss of function to oncogenic gain of function to dominant-negative effects, each influencing cancer progression in distinct ways <sup>1</sup>. Clinically, the presence of *TP53* mutations is often associated with a poor response to conventional therapies, highlighting the urgent need for innovative treatment strategies tailored to *TP53*-mutated tumors.

Acute myeloid leukemia (AML) is a devastating disease with a long-term survival rate below 30% <sup>5</sup>. While AML is a genetically heterogeneous disease, *TP53* mutations are among the most powerful risk factors in AML <sup>6-10</sup>. The World Health Organization (WHO) and the International Consensus Classification (ICC) recently updated their criteria to classify AML with *TP53* mutations as a distinct category indicating poor prognosis <sup>11,12</sup>. Previous studies have shown that AML with *TP53* mutations is often refractory to conventional chemotherapies <sup>6,7</sup>, allogeneic hematopoietic stem cell transplantation <sup>13,14</sup>, and even treatment with novel therapies such as the BCL-2 inhibitor Venetoclax <sup>15-17</sup>. Recent analysis indicates that *TP53* missense mutations prevalent in AML primarily confer a dominant-negative effect, counteracting wild-type (WT) p53 function <sup>18</sup>. Intriguingly, AML cells with *TP53* mutations often present with hematopoietic stem cell (HSC) and/or erythroid signatures, which are associated with resistance to therapy <sup>19-21</sup>.

To identify functional gene/pathway dependencies that confer fitness advantages of *TP53*-mutated AML, we performed genome-wide CRISPR/Cas9 dropout screens using isogenic *Trp53*-WT and knockout (KO) mouse AML lines. Here we show that *TP53* mutation rewires a histone gene regulatory network governed by the XPO7-NPAT pathway, creating a critical dependency in *TP53*-mutated AML cells.

#### **Methods**

For detailed methods, see Supplemental Methods.

#### Cell lines, mice and patient samples

A mouse AML line expressing the *MLL::AF9* fusion and Cas9 was previously described <sup>22</sup>. 8-12 week-old C57BL/6.*Rag2*<sup>null</sup>*Il2rg*<sup>null</sup>NOD-*Sirpa* (BRGS) mice<sup>23</sup> or NSG mice (The Jackson Laboratory, RRID: BCBC\_1262) were utilized for transplant experiments. Mice were bred and housed in individual ventilated cages, with access to autoclaved food and water, at the Kyushu University Animal Facility. All animal experiments received approval from the Institutional Animal Care and Use Committee, in accordance with national and institutional guidelines. Nineteen de novo AML, MDS, and normal donor samples were collected at Kyushu University Hospital, following protocols approved by the institutional review board. Written informed consent was obtained from all participants, in line with the Declaration of Helsinki principles.

#### Genome-wide CRISPR screen

GeCKOv2 and Brie libraries were obtained from Addgene (plasmids #1000000052 and #73632). The plasmid pool was prepared following the protocol available at Addgene's website. In brief, the sgRNA library was introduced into *Trp53*-WT or -KO mouse AML cells (1.3x10<sup>8</sup>) via

lentiviral transduction, aiming for a transduction efficiency of 30% to achieve an average coverage exceeding 500-fold. Following puromycin selection starting on day 1,  $4.0 \times 10^7$  cells were collected on day 3 to acquire input DNA. Cells were then cultured maintaining a minimum of 3 x  $10^7$  cells at all times to preserve sgRNA diversity, and collected on day 18.

#### Single-cell RNA-sequencing (scRNA-seq)

Bone marrow mononuclear cells (BMMNCs) were isolated from three AML patients and two healthy donors and processed for scRNA-seq with a Chromium Next GEM Single Cell 5' Reagent Kit v2 (10x Genomics), following the manufacturer's instructions. Constructed libraries were quantified and sequenced on a NextSeq2000 (Illumina) system.

#### Data availability

RNA-seq, ATAC-seq and scRNA-seq data were deposited in the Gene Expression Omnibus (GEO) database under accession number GSE264596.

#### **Results**

Xpo7 exhibits contrasting roles in AML cell proliferation depending on *Trp53* mutational status

To perform CRISPR/Cas9 dropout screens using AML lines with a relatively clean genetic background, we previously established AML in mice by transducing mouse bone marrow stem/progenitor cells with the *MLL::AF9* leukemia oncogene. We then established an AML line stably expressing Cas9 nuclease with functionally normal *Trp53* (mouse *TP53*) and a normal karyotype <sup>22</sup>, from which we generated a *Trp53* KO line utilizing a single guide RNA (sgRNA)

targeting Trp53. Using these isogenic lines, we performed genome-wide CRISPR-Cas9 dropout screens employing two different sgRNA libraries, GeCKO v2 <sup>24</sup> and Brie <sup>25</sup>, to identify genes/pathways whose loss renders AML cells vulnerable to Trp53KO (Figure 1A and **Supplemental Table 1**). After a 16-day culture period, sgRNAs targeting *Trp53* were highly enriched in Trp53 WT AML cells, but not on a Trp53 KO background, while those targeting Mdm2, which encodes an E3 ubiquitin-protein ligase targeting p53, were depleted only in Trp53 WT cells, attesting to the validity of our experimental system (Figure 1B, Supplemental Figure 1A-E). We then searched for genes whose sgRNAs were enriched in *Trp53* WT cells but depleted on a Trp53 KO background and identified Xpo7, a putative nuclear/cytoplasmic transporter <sup>26</sup>, at the end of the culture period (Figures 1B and 1C). Importantly, these findings were validated using two CRISPR-Cas9 screening databases of human cancers <sup>27</sup>. Dependency of these cancers on XPO7 correlated positively with TP53 dependency, as well as that of the p53 pathway genes CDKN1A, TP53BP1, ATM and CHEK2 (Figure 1D). Notably, analysis of DepMap data revealed a strong correlation between XPO7 and TP53 dependency in TP53-WT non-AML cancer cell lines, whereas TP53-WT AML lines exhibited markedly lower dependencies on both genes. (Supplemental Figures 1F and 1G). We next performed a CRISPR-Cas9 saturation mutagenesis scan <sup>28</sup> in *Trp53*-WT and -KO AML cells using a total of 1,580 sgRNAs targeting all *Xpo7* exons. Intriguingly, sgRNAs targeting *Xpo7* coding regions were significantly enriched in the Trp53 WT cells but depleted in Trp53 KO cells. By contrast, sgRNAs targeting the *Xpo7* 3'-untranslated region (3'-UTR) showed similar dependencies between Trp53-WT and -KO cells (Figures 1E and 1F). Collectively, these data suggest contrasting roles for Xpo7 in AML cell fitness depending on a cell's Trp53 status.

134

135

136

137

138

139

140

141

142

143

144

145

146

147

148

149

150

151

152

153

154

155

156

157

Xpo7 regulates nuclear abundance of p53 protein in Trp53 WT AML cells

Xpo7, a member of the exportin protein family, reportedly functions in transport of various proteins between the nucleus and cytoplasm <sup>26,29</sup> and acts as a tumor suppressor in certain solid cancers <sup>30</sup>; however, its role in AML pathogenesis remains unknown. To validate a tumor suppressive role in *Trp53* WT AML cells, we performed a second CRISPR-Cas9 dropout screen using a sgRNA library targeting 1,318 genes selected based on the initial screening results (Supplemental Table 2), with either DMSO vehicle or Nutlin-3a, an MDM2 inhibitor that stabilizes p53 protein. sgRNAs targeting Xpo7 were significantly enriched by Nutlin-3a treatment as were those targeting p53 pathway genes, including Casp9, Apaf1, Atg12, and Bax (**Figure 2A**). These results were validated by cell competition assays: cells expressing *Xpo7* sgRNA showed a proliferative advantage over non-transduced cells, an effect enhanced under Nutlin-3a treatment (Figure 2B and Supplemental Figure 2A). Growth curve analysis and Annexin V assays further demonstrated that Xpo7-depleted cells show relatively enhanced proliferation and undergo less apoptosis (Supplemental Figures 2B and 2C). Furthermore, Xpo7 KO cells were less sensitive to Nutlin-3a, as revealed by dose-response curves (Supplemental **Figure 2D**). To assess *Xpo7* depletion effects on p53-dependent transcriptional programs, we performed RNA-seq in the presence of Nutlin-3a using Xpo7-WT and -KO cells on a Trp53 WT background. Analysis of differentially-expressed genes showed marked attenuation of p53dependent transcriptional programs in the absence of *Xpo7*: namely, known *Trp53* target genes, such as Cdkn1a, Mdm2 and Pmaip1, were less induced in Xpo7 KO cells following Nutlin-3a treatment (Figure 2C), results validated by gene set enrichment analysis (GSEA) and RT-qPCR (Supplemental Figure 2E and Figure 2D). Since Xpo7 reportedly mediates protein nuclear import and/or export <sup>26,29</sup>, we hypothesized that Xpo7 modulates nuclear p53 protein levels. To test this, we assessed p53 protein distribution in nuclear and cytoplasmic fractions by Western blotting. Strikingly, nuclear p53 levels were significantly decreased in Xpo7 KO cells, with

158

159

160

161

162

163

164

165

166

167

168

169

170

171

172

173

174

175

176

177

178

179

180

effects more notable upon Nutlin-3a treatment (**Figure 2E** and **Supplemental Figure 2F**). Exportin 1 (XPO1) reportedly promotes nuclear export of p53 protein, and selinexor, an XPO1 inhibitor, suppresses tumor growth by promoting p53 nuclear retention <sup>31,32</sup>. We next asked whether Xpo7 counteracts selinexor activity in the context of p53 transport. In *Xpo7* WT cells, selinexor treatment increased p53 protein levels, effects that were less robust in *Xpo7* KO cells, suggesting that *Xpo7* promotes p53 nuclear retention in *Trp53* WT AML cells (**Figure 2F**, **Supplemental Figures 2G** and **2H**). Accordingly, *Xpo7* KO cells were less sensitive to selinexor-induced cell death, as revealed by dose-response curves (**Supplemental Figure 2I**).

To evaluate effects of Xpo7 depletion on p53 stability, we performed a fractionation assay in the presence of bortezomib, a proteasome inhibitor. Unlike untreated cells, bortezomib treatment increased nuclear p53 levels in *Xpo7* KO cells to levels comparable to those seen in *Xpo7* WT cells, and we detected cytoplasmic p53 only in *Xpo7* KO cells (**Supplemental Figure 2J**). We then conducted cycloheximide-chase assays using *Trp53* WT AML cells on either an *Xpo7* WT or KO background. p53 half-life after cycloheximide treatment was moderately reduced in *Xpo7* KO cells (3.45 vs. 2.01 hours), although the difference did not reach statistical significance under these experimental conditions (p = 0.12; **Supplemental Figures 2K** and **2L**). Collectively, these results suggest that XPO7 controls nuclear abundance of p53 protein by regulating both its nuclear import and stability.

#### XPO7 is necessary for fitness of AML cells lacking functional p53

Our CRISPR screen results suggest that *Xpo7* is required for fitness of *Trp53* KO cells, in contrast to effects seen in *Trp53* WT cells (**Figures 1C** and **E**). To validate these results, we assessed effects of *Xpo7* depletion on growth of AML cells lacking functional p53. To do so, we

knocked-out Xpo7 via lentivirus-based Crimson-tagged sgRNAs and monitored growth of AML cells lacking Trp53 (Trp53 KO) and those harboring a Trp53 R245O mutation (equivalent to TP53 R248Q in humans) with a Trp53 null allele (Trp53R245Q/-). After 12 days, Xpo7 sgRNA transduction was toxic to both Trp53 KO and Trp53<sup>R245Q/-</sup> cells (Figure 3A and Supplemental Figure 3A). We then asked if Xpo7 deletion altered cell proliferation and apoptosis using growth curve analysis and Annexin V assays, respectively (Supplemental Figures 3B and 3C). Of note, p53 R245O mutant proteins were abundant in both the nucleus and cytoplasm, regardless of *Xpo*7 status in *Trp53*<sup>R245Q/-</sup> AML cells, in the presence or absence of selinexor treatment (Supplemental Figures 3D and 3E). TP53-mutated human AML lines expressing XPO7 shRNAs also exhibited negative fitness effects across various TP53 mutation types, including missense and truncating mutations, whereas those effects were less pronounced in TP53-WT AML lines (Figure 3B and Supplemental Figure 3F). These findings in human AML cell lines contrasted with those seen in murine models, where *Xpo7* deletion enhanced leukemic growth, particularly under p53-activating conditions (Figure 2B and Supplemental Figures 2B-D). This discrepancy may reflect species-specific differences in basal p53 expression: murine Trp53-WT AML cells expressed markedly higher levels of wild-type p53 than did their human TP53-WT counterparts (Supplemental Figure 3G). Cell cycle analysis showed delays at the G1/S transition following Xpo7 depletion, suggesting that Xpo7 is necessary for cell cycling in Trp53 KO AML cells (Figure 3C). To assess effects of XPO7 depletion on growth of TP53-mutated AML cells in vivo, we transplanted HEL cells expressing either GFP-tagged XPO7 or control scrambled shRNA into irradiated mice. XPO7-deficient HEL cells were significantly less in BM than those expressing control sgRNA (Figure 3D), and mice transplanted with XPO7-deficient cells exhibited prolonged survival relative to mice receiving XPO7-intact cells (Supplemental Figure 3H).

205

206

207

208

209

210

211

212

213

214

215

216

217

218

219

220

221

222

223

224

225

226

227

Since TP53-mutated AML clones are frequently resistant to conventional chemotherapies and can outcompete TP53 WT clones during the clinical course <sup>33,34</sup>, we next asked whether *Xpo7* status alters the competitive advantage of *Trp53*-mutated AML clones (Figure 3E). To do so, we mixed Trp53 WT and Crimson-labeled Trp53 KO cells at a 9:1 ratio, cultured them in the presence of cytotoxic agents, and assessed Crimson positivity over 12 days. As expected, Trp53 KO cells outcompeted Trp53 WT cells when Xpo7 was intact, with effects more robust in the presence of cytotoxic agents; however, strikingly, those effects were not evident in the absence of *Xpo7* (Figure 3F). We next performed analogous experiments in vivo by transplanting the mixture of Trp53-WT and -KO cells into irradiated mice. On an Xpo7 WT background, Trp53 KO cells completely outcompeted Trp53 WT cells, comprising nearly 100% of BM leukemia cells; however, on a Xpo7 KO background, Trp53 KO cells failed to outcompete Trp53 WT clones and accounted for slightly over 10% of the BM leukemia burden (Figure 3G). Furthermore, mice transplanted with the mixture on an Xpo7 KO background survived longer than those transplanted with a comparable mixture on an Xpo7 WT background (Figure 3H). We validated these findings in independent murine MLL::AF9 AML lines harboring distinct Xpo7 and/or Trp53 mutations, in the presence or absence of Ara-C treatment (Supplemental Figures 3I-L). We attribute the relatively limited survival benefit shown by Xpo7 WT mice primarily to the aggressive nature of the MLL::AF9 model, which is known to induce rapid disease progression even in a *Trp53*-WT context <sup>35</sup>.

248

249

250

251

229

230

231

232

233

234

235

236

237

238

239

240

241

242

243

244

245

246

247

#### Trp53-deficient AML cells exhibit dependence on the Xpo7-Npat axis

To define mechanisms underlying negative fitness effects of *Xpo7* depletion in *Trp53* KO AML cells, we searched for Xpo7-interacting proteins whose cytoplasmic/nuclear localization was

significantly altered by Xpo7 depletion. To do so, we performed immunoprecipitation-mass spectrometry using an anti-Xpo7 antibody in Trp53 KO AML cells and identified 105 interacting proteins, with Xpo7 being the top hit (Figure 4A, Supplemental Figure 4A and Supplemental **Table 3**). Next, to identify proteins whose localization is significantly altered by Xpo7 deletion, we performed nuclear/cytoplasmic fractionation of Trp53 KO AML cells on either an Xpo7-WT or -KO background, followed by mass spectrometry. In the absence of Xpo7, 153 proteins were more prevalent in the cytoplasm and 236 in the nucleus (Supplemental Figure 4B and **Supplemental Table 4**). We then searched for Xpo7-interacting proteins that met two criteria: 1) their localization was significantly altered by Xpo7 depletion; and 2) their absence conferred negative fitness effects on Trp53 KO AML cells in CRISPR-Cas9 dropout screens (Figure 1B and Supplemental Table 1). Among 8 candidate proteins, we focused on Npat, an activator of histone transcription at the G1/S transition of the cell cycle <sup>36</sup> (Figure 4B). Npat interacted with Xpo7 (Figure 4A), and Npat localization became less nuclear after Xpo7 depletion in Trp53 KO AMLs (Figure 4B). Furthermore, sgRNAs targeting *Npat* were markedly depleted in *Trp53* KO AML cells based on our CRISPR-Cas9 screens (Supplemental Figure 1E and Supplemental **Table 1**). Intriguingly, Npat proteins were significantly induced by *Trp53* KO in AML cells (Figure 4C), as reported <sup>37</sup>. We next assessed Npat protein localization in *Trp53* KO AML cells via immunofluorescence analysis using an anti-Npat antibody. Npat-positive nuclear foci were apparent in Trp53 KO/Xpo7 WT AML cells, but their number markedly decreased in Trp53/Xpo7 double KO cells (Figures 4D and 4E). Collectively, these data indicate that Npat protein is expressed in Trp53 KO AML cells but accumulates in the nucleus to a lesser extent when *Xpo7* is also depleted.

252

253

254

255

256

257

258

259

260

261

262

263

264

265

266

267

268

269

270

271

272

273

274

275

To assess the effects of Npat depletion on AML cell growth, we established *Trp53*-WT or -KO AML cells in which a sequence encoding an HA-FKBP12<sup>F36V</sup> tag plus P2A-GFP is

knocked-in (KI) to the endogenous Npat locus of both alleles (Trp53-WTNpat\_FK2AGFP and -KO<sup>Npat\_FK2AGFP</sup>), enabling us to both trace KI clones via GFP positivity and induce Npat protein degradation by treatment with dTag<sup>V</sup>-1 ligand (**Supplemental Figure 4C**) <sup>38</sup>. Consistent with observations in Trp53 KO cells (Figure 4C), Npat expression levels were significantly higher in Trp53 KO<sup>Npat\_FK2AGFP</sup> cells at steady state, compared to Trp53 WT<sup>Npat\_FK2AGFP</sup> cells (Supplemental Figures 4D and 4E). Npat protein degradation was evident as early as 3 hours following dTAG<sup>V</sup>-1 treatment in both lines (**Supplemental Figure 4D**). Notably, Trp53 KO<sup>Npat\_FK2AGFP</sup> cells were significantly more sensitive to Npat degradation compared to *Trp53* WT<sup>Npat\_FK2AGFP</sup> cells, as demonstrated by the dose-response curve (Figure 4F). We further validated the negative effects of Npat depletion on the fitness of Trp53-deficient AML cells by competition assays: Trp53 KO<sup>Npat\_FK2AGFP</sup> cells exhibited a proliferative disadvantage over Trp53KO cells in the presence of dTAGV-1 (Supplemental Figure 4F). Xpo7 overexpression did not rescue the growth-suppressive effects of Npat depletion, suggesting that Npat functions downstream of Xpo7 (Supplemental Figure 4G). Similarly, HEL cells showed significantly less growth when NPAT levels were knocked down by NPAT shRNA (Supplemental Figure 4H). dTag<sup>V</sup>-1-mediated Npat protein degradation led to an increase in cells at G0/G1 (**Figure 4G**), followed by apoptosis (Figure 4H). To validate these findings in vivo, we transplanted irradiated mice with Trp53 KO<sup>Npat\_FK2AGFP</sup> cells, and then treated mice with either dTag<sup>V</sup>-1 or negative control ligand for over a week (Figure 4I). Mice treated with dTag<sup>V</sup>-1 ligand exhibited relatively decreased BM leukemic burden (Figure 4J), robust Npat degradation (Supplemental Figure 4I), and prolonged survival (Figure 4K) relative to mice treated with negative control ligand.

276

277

278

279

280

281

282

283

284

285

286

287

288

289

290

291

292

293

294

295

296

297

298

Npat depletion disrupts genomic integrity in Trp53-deficient AML cells

We next examined molecular mechanisms underlying growth suppressive effects caused by Npat depletion in *Trp53* KO AML cells. To identify mRNAs downregulated following Npat depletion, we first performed RNA-seq using *Trp53*-WT or -KO<sup>Npat\_FK2AGFP</sup> AML cells, with or without dTAG<sup>V</sup>-1 treatment. That analysis revealed a marked reduction in mRNA levels of canonical histone cluster genes three hours after dTAG<sup>V</sup>-1 treatment, predominantly in *Trp53* KO cells (**Figure 5A**). Consequently, Gene Ontology (GO) analysis showed that mRNA levels of genes associated with nucleosome assembly pathways were significantly altered following Npat depletion (**Figure 5B**).

To assess both local and global chromatin accessibility in the presence or absence of Npat, we performed ATAC-Seq (assay for transposase-accessible chromatin with high-throughput sequencing) with or without dTAGV-1 treatment. While genome-wide proportions of sub/mono-nucleosomes were barely changed after dTAGV-1 treatment in *Trp53* WT cells, their proportions markedly increased in *Trp53* KO cells, accompanied by a decreased proportion of larger nucleosomes (**Figure 5C**). These findings suggest that transposase-accessibility was markedly enhanced by global histone depletion following Npat inactivation in *Trp53* KO cells. Accordingly, the number of distinct ATAC-seq signal peaks of nuclear DNA was significantly reduced, and a more diffuse pattern of transposase integration increased across the genome following dTAGV-1 treatment in *Trp53* KO cells (**Figures 5D** and **5E**). Collectively, these results indicate that Npat depletion initially decreases transcription of canonical histones, followed by a global loss of histones and a genome-wide increase in nucleosome-free DNA, with these effects being particularly pronounced in p53-deficient cells.

Considering that Npat depletion compromises genomic integrity in *Trp53* KO AML cells (**Figures 5C-E**) and that *TP53*-deficient cells are reportedly vulnerable to replication stress induced by Wee1 inhibition<sup>39</sup>, we hypothesized that combining Wee1 inhibition with Npat

depletion would induce replication catastrophe in *Trp53* KO AML cells (**Supplemental Figure 5A**). *Trp53* KO<sup>Npat\_FK2AGFP</sup> AML cells treated with a negative control ligand showed weak γH2AX signals, a marker of DNA double-strand breaks and genomic instability. In contrast, dTAG<sup>V</sup>-1 treatment induced γH2AX signals even in vehicle-treated cells, an effect greatly enhanced by treatment with Adavosertib, a Wee1inhibitor (**Figure 5F**). We next treated *Trp53*-WT<sup>Npat\_FK2AGFP</sup> and -KO<sup>Npat\_FK2AGFP</sup> cells with either DMSO, or Adavosertib, with or without 50 nM dTAG<sup>V</sup>-1 pretreatment, and generated dose-response curves. Strikingly, dTAG<sup>V</sup>-1-treated *Trp53* KO<sup>Npat\_FK2AGFP</sup> cells were significantly more sensitive to Adavosertib than *Trp53* WT<sup>Npat\_FK2AGFP</sup> cells (**Figure 5G**). Combined dTAG<sup>V</sup>-1 and Adavosertib treatment markedly induced G1/S cell cycle arrest and subsequent apoptosis in *Trp53* KO AML cells (**Supplemental Figures 5B** and **5C**). Importantly, apoptosis was induced more profoundly in *Trp53* KO cells than in *Trp53* WT cells following Npat depletion, with effects further enhanced by Adavosertib treatment (**Supplemental Figure 5C**).

XPO7 and NPAT are predominantly expressed in *TP53*-mutated human AML cases

To further assess the significance of XPO7/NPAT expression in *TP53*-mutated human AML cases, we evaluated *XPO7* and *NPAT* mRNA levels in primary human AML samples using publicly available datasets. Both *XPO7* and *NPAT* mRNA levels were significantly higher in *TP53*-mutated AML cases than in cases with WT *TP53* in both TCGA <sup>8</sup> and BeatAML <sup>40</sup> cohorts (**Figure 6A**). Their expression was particularly high in acute erythroid leukemia (AEL) cases, in which *TP53* mutations are frequent, in two independent cohorts <sup>40,41</sup> (**Supplemental Figures 6A** and **6B**). Interestingly, while leukemic/pre-leukemic cells from *TP53*-mutated AML and myelodysplastic syndrome (MDS) often exhibit a complex karyotype, chromosomes 8 and 11q,

respective locations of *XPO7* and *NPAT*, are frequently amplified in both AML and MDS cases with a *TP53* mutations (**Supplemental Figure 6C**). Western blots showed markedly high expression of NPAT and XPO7 proteins in *TP53*-mutated AML cases relative to cases with intact *TP53* or to mononuclear cells from normal BM (**Figure 6B** and **Supplemental Table 5**).

346

347

348

349

350

351

352

353

354

355

356

357

358

359

360

361

362

363

364

365

366

367

368

369

To assess intra-patient profiles of NPAT/XPO7 mRNA expression and their correlation with TP53 mutational status at single-cell levels, we performed scRNA-seq with copy number alteration (CNA) analysis using BM cells from two TP53-mutated AML cases, both carrying complex karyotypes (Figure 6C). UMAP analysis of BMMNCs revealed seven clusters, each representing a distinct lineage (Figure 6D, Supplemental Figures 7A and 7B). Among a total of 32,927 cells analyzed, 8,826 harbored no CNAs, while 24,101 exhibited multiple CNAs, indicative of TP53 deficiency (Figure 6E and Supplemental Figure 7C). CNAs were evident exclusively in the hematopoietic stem-progenitor cell (HSPC) and erythroblast clusters (Figure **6E**), and, intriguingly, both XPO7 and NPAT were predominantly co-expressed in these clusters (Figure 6F). Furthermore, XPO7 and NPAT co-expressing cells showed higher LSC (leukemia stem cell) and erythroid scores, both of which reportedly indicate TP53 deficiency in AML cells (**Figure 6G**) <sup>20,42</sup>. These observations were supported by analysis of a public bulk RNA-seq dataset, which showed elevated expression of both XPO7 and NPAT in samples with higher erythroid or LSC signatures (Supplemental Figures 7D). We also performed scRNA-seq in BM cells from a TP53-WT AML case and two healthy donors, followed by combined comparable analysis (Supplemental Figure 7E). Consistent with bulk RNA-seq and Western blot results (Figures 6A and 6B), both XPO7 and NPAT were expressed at lower levels in the TP53-WT compared to the TP53-mutated case (Supplemental Figure 7F), findings validated by analysis of publicly available RNA-seq data from isogenic TP53-WT and mutant human AML lines (Supplemental Figure 7G). In the healthy donor samples, XPO7 expression was highest in

erythroid-lineage cells—particularly at terminal stages of differentiation—whereas *NPAT* expression was relatively enriched in lymphoid populations (**Supplemental Figure 7F**).

#### Functional implications of XPO7 and NPAT depletion in AML

To investigate the potential impact of XPO7 and NPAT inhibition on normal hematopoiesis and AML progression, we employed in vitro colony formation assays and patient-derived xenotransplantation (PDX) models. CD34+ HSPCs derived from mobilized peripheral blood of three healthy donors were transduced with GFP-tagged shRNA targeting *XPO7*, *NPAT*, or a scrambled control. GFP-positive cells were sorted and evaluated for progenitor activity using colony formation assays (**Supplemental Figure 8A**). While *XPO7* knockdown had minimal effects on the formation of erythroid and myeloid colonies, *NPAT* knockdown partially reduced colony numbers in both lineages, with a relatively greater impact on erythroid colonies (**Supplemental Figure 8B**). We next conducted similar analysis of primary AML samples (*TP53*-WT: n = 3; *TP53*-mutated: n = 4). Consistent with results seen in human AML lines, depletion of either *XPO7* or *NPAT* impaired colony formation, particularly in *TP53*-mutated cases (**Supplemental Figure 8C**).

We further investigated effects of *XPO7* and *NPAT* depletion on leukemia progression in vivo using PDX models established from five AML patients—two with *TP53* mutations and three with WT *TP53*. AML cells were transduced with GFP-tagged shRNA targeting *XPO7*, *NPAT*, or a scrambled control and transplanted into irradiated immune-compromised mice (**Figure 6H**). In the *TP53* WT AML cohort, *NPAT* depletion, but not *XPO7* depletion, attenuated leukemia growth. By contrast, in the *TP53*-mutated AML cohort, depletion of either *NPAT* or *XPO7* significantly impaired leukemia growth in vivo, as evidenced by reduced leukemic burden

in BM and peripheral blood (PB) at two and four months post-transplantation, respectively (**Figure 6I**, **Supplemental Figures 8D** and **8E**). To evaluate potential effects of *XPO7* and *NPAT* depletion on LSC activity, we transduced two *TP53*-WT and three *TP53*-mutant primary AML samples with control, *XPO7*, or *NPAT* shRNAs and monitored CD34\*CD38-GFP+ cell frequency over time in vitro. We observed a progressive decline in the proportion of *XPO7*- or *NPAT*-depleted cells within the LSC-enriched fraction, particularly in *TP53*-mutated cases (**Supplemental Figure 8F**). Furthermore, limiting dilution transplantation assays using CD34\*CD38-GFP+ cells demonstrated significantly decreased engraftment following either *XPO7* or *NPAT* depletion, supporting a role for the XPO7-NPAT axis in maintaining LSC activity in *TP53*-mutated AML (**Supplemental Figure 8G**).

#### **Discussion**

In eukaryotic cells, macromolecule transport between the nucleus and cytoplasm is mediated Ran-dependently by Karyopherin-β family proteins through the nuclear pore complex <sup>43</sup>. XPO7 reportedly functions as a "biportin" mediating both cargo import and export <sup>26,29,30,43,44</sup>. Given that 1) nuclear p53 protein levels significantly decreased in *Xpo7*-deficient AML cells despite unchanged *Trp53* mRNA levels and 2) *Xpo7* depletion antagonized Selinexor activity (**Figure 2**), we propose that Xpo7 regulates p53 nuclear import via a dual mechanism: directly, through interaction with p53, and indirectly, by modulating factors that influence p53 stability. While our findings indicate that *XPO7* loss diminishes nuclear p53 accumulation and attenuates canonical p53 target gene expression, we acknowledge that nuclear localization alone may not fully account for the observed phenotypic effects. Notably, *Xpo7*-deficient cells treated with Nutlin-3a retain nuclear p53 levels higher than those in untreated controls yet display reduced

transcriptional output and diminished growth suppression (**Figure 2**). These observations suggest that additional factors—such as post-translational regulation of p53 activity or parallel XPO7-dependent pathways—may also contribute to the observed phenotype in AML.

416

417

418

419

420

421

422

423

424

425

426

427

428

429

430

431

432

433

434

435

436

XPO7 and NPAT expression is higher in TP53-mutated AML cells than in cells with intact TP53, based on publicly available datasets and our own data, with findings validated in individual patients at the single-cell level (Figure 6 and Supplemental Figure 7). TP53-mutated AML cases reportedly exhibit an erythroid signature, as do most AEL cases 41,42,45. It is, however, unclear whether the "erythroid signature", including high XPO7/NPAT expression reported here, is driven by instructive or permissive effects of TP53 deficiency. While underlying mechanisms remain unclear, we propose two possibilities that are not mutually exclusive: 1) TP53-mutant AML may adopt erythroid-biased transcriptional programs, and given that XPO7 is highly expressed in normal erythroid precursors, its elevated expression in TP53mutant AML may reflect lineage bias or ontogenetic mimicry; 2) p53 dysfunction may promote XPO7 and NPAT upregulation, either directly or indirectly, through mechanisms that are independent of lineage differentiation. Supporting this second possibility, NPAT has been reported to function downstream of the p53-p21 axis <sup>36</sup>. Further studies are needed to delineate whether high XPO7/NPAT expression in TP53-mutant AML primarily reflects lineage context or represents an acquired dependency linked to TP53 loss.

In summary, using unbiased functional genomic approaches along with transcriptomic and proteomic analyses, we have identified the histone gene regulatory network governed by the XPO7/NPAT axis as a key vulnerability in *TP53*-mutated AML.

Antl	ore,	Disc	losures
AIIII	1018	17180	108111.68

The authors declare no competing interests.

#### **Authors' Contributions**

Conceptualization, T.M.; methodology, Y.S., T.Y., D.B. and S.O.; Investigation, Y.S. and T.Y.; writing—original draft, Y.S. and T.M.; writing—review & editing, T.M.; funding acquisition, Y.S., T.Y., S.O., K.A. and T.M.; resources, K.A. and T.M.; supervision, S.O., K.A. and T.M.

#### Acknowledgments

We thank the members of the Department of Medicine and Biosystemic Science and the Division of Precision Medicine at Kyushu University for assistance and helpful discussion, Takeshi Iwasaki for expert advice and support, and Elise Lamar for critical reading of the manuscript. This work is supported in part by a JSPS Grant-in-Aid for JSPS Fellows (19J01412), a JSPS Grant-in-Aid for Young Scientists (18K16089), a JSPS Grant-in-Aid for Young Scientists (22K16303), a grant from SENSHIN Medical Research Foundation, Nippon Shinyaku Research Grant, a grant from YOKOYAMA Foundation for Clinical Pharmacology, Grant of The Clinical Research Promotion Foundation, a grant from the Shinnihon Foundation of Advanced Medical Treatment Research (to Y.S.), a JSPS Grant-in-Aid for Young Scientists (19K17859) (to T.Y.), a JSPS Grant-in-Aid for Scientific Research (S)(16H06391) (to K.A.), a JSPS Grant-in-Aid for Scientific Research (A) (17H01567), a JSPS Grant-in-Aid for Scientific Research (S) (20H05699), AMED under grant number 18063889, Takeda COCKPI-T® Funding (to T.M.).

#### **Supplemental Information**

- Supplemental Documents: Supplemental Methods and Supplemental Figures 1 to 9
- Supplemental Tables 1 to 5

#### References

459

462

463

466

467

477

478

- 1. Kastenhuber ER, Lowe SW. Putting p53 in Context. *Cell.* 2017;170(6):1062-1078.
- 2. Levine AJ. p53: 800 million years of evolution and 40 years of discovery. *Nat Rev Cancer*. 2020;20(8):471-480.
  - 3. Mendiratta G, Ke E, Aziz M, Liarakos D, Tong M, Stites EC. Cancer gene mutation frequencies for the U.S. population. *Nat Commun*. 2021;12(1):5961.
- 4. Giacomelli AO, Yang X, Lintner RE, et al. Mutational processes shape the landscape of TP53 mutations in human cancer. *Nat Genet*. 2018;50(10):1381-1387.
- 5. Shallis RM, Wang R, Davidoff A, Ma X, Zeidan AM. Epidemiology of acute myeloid leukemia: Recent progress and enduring challenges. *Blood Rev.* 2019;36:70-87.
- 6. Bejar R, Stevenson K, Abdel-Wahab O, et al. Clinical effect of point mutations in myelodysplastic syndromes. *N Engl J Med*. 2011;364(26):2496-2506.
- 7. Rücker FG, Schlenk RF, Bullinger L, et al. TP53 alterations in acute myeloid leukemia with complex karyotype correlate with specific copy number alterations, monosomal karyotype, and dismal outcome. *Blood.* 2012;119(9):2114-2121.
  - 8. Cancer Genome Atlas Research N, Ley TJ, Miller C, et al. Genomic and epigenomic landscapes of adult de novo acute myeloid leukemia. *N Engl J Med*. 2013;368(22):2059-2074.
- 9. Papaemmanuil E, Gerstung M, Bullinger L, et al. Genomic Classification and Prognosis in Acute Myeloid Leukemia. *N Engl J Med*. 2016;374(23):2209-2221.
- 481 10. Grob T, Al Hinai ASA, Sanders MA, et al. Molecular characterization of mutant TP53 acute myeloid leukemia and high-risk myelodysplastic syndrome. *Blood*. 2022;139(15):2347-483 2354.
- 484 11. Khoury JD, Solary E, Abla O, et al. The 5th edition of the World Health Organization 485 Classification of Haematolymphoid Tumours: Myeloid and Histiocytic/Dendritic Neoplasms. 486 *Leukemia*. 2022;36(7):1703-1719.
- 487 12. Arber DA, Orazi A, Hasserjian RP, et al. International Consensus Classification of
  488 Myeloid Neoplasms and Acute Leukemias: integrating morphologic, clinical, and genomic data.
  489 *Blood.* 2022;140(11):1200-1228.
- Lindsley RC, Saber W, Mar BG, et al. Prognostic Mutations in Myelodysplastic Syndrome after Stem-Cell Transplantation. *N Engl J Med*. 2017;376(6):536-547.
- 492 14. Yoshizato T, Nannya Y, Atsuta Y, et al. Genetic abnormalities in myelodysplasia and 493 secondary acute myeloid leukemia: impact on outcome of stem cell transplantation. *Blood*. 494 2017;129(17):2347 - 2358.
- 15. Nechiporuk T, Kurtz SE, Nikolova O, et al. The TP53 Apoptotic Network Is a Primary Mediator of Resistance to BCL2 Inhibition in AML Cells. *Cancer Discov.* 2019.
- 16. DiNardo CD, Jonas BA, Pullarkat V, et al. Azacitidine and Venetoclax in Previously Untreated Acute Myeloid Leukemia. *N Engl J Med*. 2020;383(7):617-629.
- Shimony S, Garcia JS, Keating J, et al. Molecular ontogeny underlies the benefit of adding venetoclax to hypomethylating agents in newly diagnosed AML patients. *Leukemia*.

501 2024.

- 18. Boettcher S, Miller PG, Sharma R, et al. A dominant-negative effect drives selection of 502 TP53 missense mutations in myeloid malignancies. Science. 2019;365(6453):599-604. 503
- Kuusanmaki H, Dufva O, Vaha-Koskela M, et al. Erythroid/megakarvocytic 504
- differentiation confers BCL-XL dependency and venetoclax resistance in acute myeloid 505 leukemia. Blood. 2023;141(13):1610-1625. 506
- Zeng AGX, Iacobucci I, Shah S, et al. Precise single-cell transcriptomic mapping of 507 normal and leukemic cell states reveals unconventional lineage priming in acute myeloid 508
- leukemia. bioRxiv. 2023. 509
- Mohanty V, Baran N, Huang Y, et al. Transcriptional and phenotypic heterogeneity 510 underpinning venetoclax resistance in AML. bioRxiv. 2024. 511
- Yamauchi T, Masuda T, Canver MC, et al. Genome-wide CRISPR-Cas9 Screen 512 22.
- Identifies Leukemia-Specific Dependence on a Pre-mRNA Metabolic Pathway Regulated by 513
- DCPS. Cancer Cell. 2018;33(3):386-400.e385. 514
- Yamauchi T, Takenaka K, Urata S, et al. Polymorphic Sirpa is the genetic determinant 515
- for NOD-based mouse lines to achieve efficient human cell engraftment. Blood. 516
- 2013;121(8):1316-1325. 517
- Sanjana NE, Shalem O, Zhang F. Improved vectors and genome-wide libraries for 518
- CRISPR screening. *Nat Methods*. 2014;11(8):783-784. 519
- Doench JG, Fusi N, Sullender M, et al. Optimized sgRNA design to maximize activity 520 25.
- and minimize off-target effects of CRISPR-Cas9. *Nature Biotechnology*. 2016;34(2):184-191. 521
- Aksu M, Pleiner T, Karaca S, et al. Xpo7 is a broad-spectrum exportin and a nuclear 522 import receptor. J Cell Biol. 2018;217(7):2329-2340. 523
- 27. Pacini C, Dempster JM, Boyle I, et al. Integrated cross-study datasets of genetic 524
- dependencies in cancer. Nature Communications. 2021;12(1). 525
- Shi J, Wang E, Milazzo JP, Wang Z, Kinney JB, Vakoc CR. Discovery of cancer drug 526 527
  - targets by CRISPR-Cas9 screening of protein domains. Nat Biotechnol. 2015;33(6):661-667.
- Markiewicz Ł, Uśpieński T, Baran B, Niedziółka SM, Niewiadomski P. Xpo7 negatively 528
- 529 regulates Hedgehog signaling by exporting Gli2 from the nucleus. Cellular Signalling.
- 2021;80:109907. 530
- 531 30. Innes AJ, Sun B, Wagner V, et al. XPO7 is a tumor suppressor regulating p21(CIP1)-
- dependent senescence. Genes Dev. 2021;35(5-6):379-391. 532
- 31. Kanai M, Hanashiro K, Kim S-H, et al. Inhibition of Crm1-p53 interaction and nuclear 533
- export of p53 by poly(ADP-ribosyl)ation. Nature Cell Biology. 2007;9(10):1175-1183. 534
- Walker CJ, Oaks JJ, Santhanam R, et al. Preclinical and clinical efficacy of XPO1/CRM1 535
- inhibition by the karyopherin inhibitor KPT-330 in Ph+ leukemias. Blood. 2013;122(17):3034-536 537 3044.
- 33. Wong TN, Ramsingh G, Young AL, et al. Role of TP53 mutations in the origin and 538
- evolution of therapy-related acute myeloid leukaemia. *Nature*. 2015;518(7540):552-555. 539
- 34. Guess T, Potts CR, Bhat P, et al. Distinct Patterns of Clonal Evolution Drive 540
- Myelodysplastic Syndrome Progression to Secondary Acute Myeloid Leukemia. Blood Cancer 541 Discovery. 2022;3(4):316-329. 542
- 35. Somervaille TCP, Cleary ML. Identification and characterization of leukemia stem cells 543 in murine MLL-AF9 acute myeloid leukemia. Cancer Cell. 2006;10(4):257-268. 544
- Zhao J, Kennedy BK, Lawrence BD, et al. NPAT links cyclin E–Cdk2 to the regulation 545
- of replication-dependent histone gene transcription. Genes & Development. 2000;14(18):2283-546
- 2297. 547

- 548 37. Pirngruber J, Johnsen SA. Induced G1 cell-cycle arrest controls replication-dependent
- histone mRNA 3' end processing through p21, NPAT and CDK9. Oncogene. 2010;29(19):2853-
- 550 2863.

- Nabet B, Ferguson FM, Seong BKA, et al. Rapid and direct control of target protein
- levels with VHL-recruiting dTAG molecules. *Nature Communications*. 2020;11(1):4687.
- 553 39. Pilie PG, Tang C, Mills GB, Yap TA. State-of-the-art strategies for targeting the DNA
- damage response in cancer. *Nat Rev Clin Oncol*. 2019;16(2):81-104.
- 555 40. Bottomly D, Long N, Schultz AR, et al. Integrative analysis of drug response and clinical outcome in acute myeloid leukemia. *Cancer Cell*. 2022;40(8):850-864 e859.
- 557 41. Iacobucci I, Wen J, Meggendorfer M, et al. Genomic subtyping and therapeutic targeting of acute erythroleukemia. *Nature Genetics*. 2019;51(4):694 704.
- 559 42. Rodriguez-Meira A, Norfo R, Wen S, et al. Single-cell multi-omics identifies chronic inflammation as a driver of TP53-mutant leukemic evolution. *Nature Genetics*. 2023.
- 561 43. Wing CE, Fung HYJ, Chook YM. Karyopherin-mediated nucleocytoplasmic transport. 562 *Nat Rev Mol Cell Biol.* 2022;23(5):307-328.
- 563 44. Li L-Z, Yang K, Jing Y, et al. CRISPR-based screening identifies XPO7 as a positive regulator of senescence. *Protein & Cell*. 2023.
- Takeda J, Yoshida K, Nakagawa MM, et al. Amplified EPOR/JAK2 Genes Define a Unique Subtype of Acute Erythroid Leukemia. *Blood Cancer Discov.* 2022;3(5):410-427.
- 567 46. Colic M, Wang G, Zimmermann M, et al. Identifying chemogenetic interactions from CRISPR screens with drug Z. *Genome Med.* 2019;11(1):52.
- 569 47. Wu T, Hu E, Xu S, et al. clusterProfiler 4.0: A universal enrichment tool for interpreting omics data. *Innovation (Camb)*. 2021;2(3):100141.
- 571 48. Hao Y, Stuart T, Kowalski MH, et al. Dictionary learning for integrative, multimodal and scalable single-cell analysis. *Nat Biotechnol*. 2024;42(2):293-304.

#### Figure legends

575

576

577

578

579

580

581

582

583

584

585

586

587

588

589

590

591

592

593

594

595

596

Figure 1. Genome-wide CRISPR-Cas9 screens identify contrasting *Xpo7* functions in AML fitness depending on *TP53* status.

(A) Schematic representation of CRISPR-Cas9 screens. Indicated *Trp53*-WT or -KO isogenic mouse MLL:: AF9 AML lines stably expressing Cas9 were transduced with the GeCKO or Brie library, selected with puromycin, and cultured 16 days. sgRNA abundance before and after culture was assessed as described <sup>22</sup>. (B) A Z-score, representing the difference in gene dependency between Trp53-WT and -KO screens, was calculated for each gene, and a dot graph representing Z-scores in both screens—Brie (X-axis) and GeCKOv2 (Y-axis)—for each gene was generated. Red, genes with statistically significant Z-scores (FDR < 0.05) in both screens. (C) Graphs showing read counts of individual sgRNAs targeting *Xpo7* in the GeCKOv2 (top) or Brie (bottom) screen on either a Trp53-WT (blue) or -KO (red) background. (D) Dot graph showing correlation between gene dependency and TP53 dependency for each gene. Sample Pearson correlation coefficients are calculated based on Sanger (X-axis) and Avana (Y-axis) DepMap datasets. Red, genes significantly correlated with TP53 dependency (P value  $< 10^{-15}$ ) across both datasets. (E) CRISPR-Cas9 saturation mutagenesis scan targeting Xpo7 exons using Trp53-WT (blue) and -KO (red) AML cells. All NGG-restricted sgRNAs (n = 1,747) were transduced and dropout screens were performed. Read counts from days 17 and 3 were normalized to non-targeting guides and log2 fold-change in guide abundance was calculated. (F) Box plots show log2 fold-changes in guide abundance for both Xpo7 coding sequence (CDS) and 3'UTR regions in Trp53-WT (blue) and -KO (red) cells.

Figure 2. Xpo7 functions as a Trp53-dependent tumor suppressor in Trp53 WT AML cells.

598

599

600

601

602

603

604

605

606

607

608

609

610

611

612

613

614

615

616

617

(A) Results of a second dropout screen targeting 1,000 selected genes in the presence of the MDM2 inhibitor Nutlin-3a or DMSO vehicle. Genes with sgRNA abundance significantly altered by Nutlin-3a treatment were assessed using the drugZ program <sup>46</sup>. Red dots, genes showing statistically significant changes (FDR < 0.01). (B) Xpo7-WT and -KO mouse AML cells were mixed 1:1 and cultured with either DMSO or 5 µM Nutlin-3a, and the fraction of Xpo7 KO cells labeled with Crimson fluorescent protein was measured at indicated time points based on FACS. Crimson positivity at each time point was normalized to that on day 0. Empty vector, control cells. Each condition was assessed in triplicate, and data are shown as means  $\pm$ SD. (C) RNA-seq was performed in triplicate after 24h of Nutlin-3a treatment using Xpo7-WT and -KO mouse AML cells. Heatmap shows scaled mean TPM (transcript per million) values of 40 p53 target genes. (D) Xpo7-WT and -KO AML cells were treated 24h with DMSO or 5 μM Nutlin-3a, and Cdkn1a, Mdm2 and Trp53 mRNA levels relative to Gapdh were measured by RTqPCR. Bar graphs show mRNA levels normalized to those seen in DMSO-treated WT cells for each gene. Each condition was assessed in triplicate, and data are shown as means  $\pm$  SD. P values were calculated using an unpaired t-test. (E) Cytoplasmic (Cyto) or nuclear (Nuc) p53 protein from Xpo7-WT and -KO lines treated 24h with 10 μM Nutlin-3a was assessed by Western blot. (F) Xpo7-WT and -KO lines were treated with 100 nM selinexor, and whole-cell lysates were analyzed by Western blot for p53 and Xpo7 proteins. β-actin served as loading control.

Figure 3. XPO7 is necessary for fitness of AML cells lacking functional	ess of AML cells lacking functional page 1	itness of	ecessary for	<i>XPO7</i> i	Figure 3.	]
---	--	-----------	--------------	---------------	-----------	---

619

620

621

622

623

624

625

626

627

628

629

630

631

632

633

634

635

636

637

638

639

640

641

(A) Xpo7-WT and -KO mouse AML cells on either a Trp53-KO (left) or -mutant (right) background were mixed 1:1, and the fraction of *Xpo7* KO cells, as indicated by Crimson labeling, was measured by FACS at indicated time points. Crimson positivity was normalized to that seen on day 0. Empty vector, control cells. Each condition was assessed in triplicate, and data are shown as means. (B) Human AML lines harboring TP53 mutations were transduced with a lentivirus vector harboring indicated shRNAs plus a GFP cassette and cultured for 12 days. GFP-positivity at indicated time points, as assessed by FACS, was normalized to that seen on day 0 (2 days after transduction). Scrambled shRNA cells served as control. Each condition was assessed in triplicate, and data are represented as means  $\pm$  SD. (C) Cell cycle analysis was performed in Xpo7-WT and -KO mouse AML cells on a Trp53 KO background. Bars show proportions of cells at each cell cycle stage. Data are shown as means ± SD of three independent experiments. P values were calculated using an unpaired t-test. (D) HEL cells were transduced with a lentivirus vector encoding indicated shRNAs plus a GFP cassette at a transduction efficiency of 30% and transplanted into immunocompromised mice (5-6 mice per group). Proportions of GFP-positive cells in hCD45+ cell fractions in BM were assessed by FACS 21 days later. Dot graphs showing GFP positivity on day 21 normalized to that seen in transplanted grafts. P values were calculated using an unpaired t-test. (E) Schematic representations of in vitro and in vivo competition assays. Trp53 WT and Crimson-labeled Trp53 KO cells were mixed 9:1 on either an Xpo7 WT or Xpo7 KO background and either cultured with cytotoxic agents or transplanted into immunocompromised mice. (F) Cell mixtures on either an Xpo7 WT (left) or KO (right) background were cultured for 12 days with either vehicle (DMSO), Daunorubicin (10 nM), Cytarabine (50 nM), or Etoposide (20 nM), and GFP positivity assessed by FACS at indicated time points. Each condition was assessed in triplicate, and data are shown

as means $\pm$ SD. (G) Cell mixtures on either an $Xpo/W1$ or KO background were prepared as in
(F) and transplanted into irradiated mice (n=4 per experimental group). GFP positivity in BM
was assessed 21 days later by FACS. Bar graphs show proportions of GFP-positive cells (Trp53
KO cells) on either an $\textit{Xpo7-WT}$ (grey) or -KO (red) background. Data are shown as means $\pm$
SD. P values were calculated using an unpaired t-test. <b>(H)</b> Cell mixtures on either an <i>Xpo7</i> WT
or KO background were transplanted into irradiated mice (n=5 per group), and survival curves
generated. P values were calculated using weighted Log-rank tests.

(A) Volcano plot displaying results of triplicate IP/mass spectrometry analyses of Xpo7 binding proteins in Trp53 KO mouse AMLs. Y-axis shows negative log2 FDR values, which represent reproducibility of events among three independent experiments, and X-axis indicates log2 ratio of normalized protein abundance between anti-Xpo7 antibody and control Ig IPs. Red, significantly enriched proteins (FDR < 0.01). (B) Volcano plot displaying results of triplicate mass spectrometry analyses of nuclear or cytoplasmic protein fractions from Trp53 KO versus Trp53/Xpo7 DKO mouse AML cells. Y-axis shows negative log2 P values; X-axis indicates log2 ratio of normalized cytoplasmic protein abundance on Xpo7-WT and -KO backgrounds. Circle size indicates the absolute β-score and represents the degree of fitness effects of respective genes detected in the GeCKO v2 CRISPR/Cas9 dropout screen (Fig.1). Red, proteins whose localization was significantly altered in the absence of Xpo7 (FDR < 0.01). (C) Npat protein levels in Trp53-WT and -KO mouse AML cells, based on Western blotting using anti-Npat antibody. Npat KO lines served as negative controls, and β-actin as a loading control. (D) Npat protein (red) levels and localization, as assessed by immunofluorescence in Trp53 KO AML cells on either an Xpo7-WT (left) or -KO (right) background. Hoechst staining (blue) indicates nuclei. (E) Npat foci were counted in Trp53 KO AML cells on either an Xpo7-WT (left) or -KO (right) background. P values were calculated using an unpaired t-test. (F) Trp53 WTNpat\_FK2AGFP and Trp53 KO<sup>Npat\_FK2AGFP</sup> lines were treated with dTAG<sup>V</sup>-1 at indicated doses, and cell counts determined 72h later. Counts at each dose were normalized to those of the DMSO control, and dose response curves were generated. Each condition was assessed in triplicate. (G) Cell cycle analysis was performed using Trp53 KONpat\_FK2AGFP AML cells following either 500 nM dTagV-1 or NEG treatment. Bars indicate proportions of cells at each cell cycle stage. Data are shown as means of three independent experiments  $\pm$  SD. P values were calculated using an unpaired t-test.

Figure 4. The Xpo7- Npat axis is a functional vulnerability in *Trp53*-deficient AML cells.

650

651

652

653

654

655

656

657

658

659

660

661

662

663

664

665

666

667

668

669

670

671

672

(H) Proportions of apoptotic cells were assessed by Annexin V staining following control
DMSO or 500 nM dTAG <sup>v</sup> -1 treatment. P values were calculated using an unpaired t-test. (I)
Schematic representations of in vivo experiments. Trp53 KONpat_FK2AGFP AML cells were
transplanted into immunocompromised mice, and 2 weeks later mice were treated with either
dTag <sup>V</sup> -1 or NEG ligand. (J) Proportions of GFP-positive cells in CD45+ cell fractions in BM
were assessed by FACS after a week of drug treatment. Five mice per condition were analyzed. P
values were calculated using an unpaired t-test. (K) Immunocompromised mice were
transplanted with $\mathit{Trp53}~\mathrm{KO^{Npat\_FK2AGFP}}$ AML cells, and a week later, treated with either $\mathrm{dTag^V-1}$
or NEG ligand for 7 days (n=5 per group). Survival curves and P values were calculated using
weighted log-rank tests.

Figure 5. Npat depletion in *Trp53* KO AML cells decreases histone transcription and compromises genome integrity.

687

688

689

690

691

692

693

694

695

696

697

698

699

700

701

702

703

704

705

706

707

708

709

(A) Volcano plot showing RNA-seq analysis of Trp53 WTNpat\_FK2AGFP (left) and Trp53 KO<sup>Npat\_FK2AGFP</sup> (right) AML cells treated three hours with or without dTAG<sup>V</sup>-1. Y-axis shows negative log2 FDR values; X-axis shows log2 ratio of normalized read counts from before to after dTAG<sup>V</sup>-1 treatment. Red, canonical histone genes localized in histone clusters. (B) Gene Ontology (GO) analysis on differentially expressed genes using clusterProfiler package <sup>47</sup>. (C) Proportions of both sub/mono-nucleosomes and larger nucleosomes (>di-nucleosomes), as assessed by ATAC-seq fragment size distribution. Box plots illustrate proportions of each nucleosome fraction of Trp53-WT or -KO AML cells with or without 12 hours dTAGV-1 treatment. (D) Bar graphs display the count of ATAC-seq signal peaks annotated using MACS2 software, measured in Trp53-WT or -KO AML cells with or without 12 hours dTAG<sup>V</sup>-1 treatment. (E) Heatmap illustrating ATAC-seq signal intensities around transcription start sites (TSS) within a  $\pm$  3kb range, captured in *Trp53*-WT or -KO AML cells with or without 12 hours dTAG<sup>V</sup>-1 treatment. (F) γH2AX protein (red) signal intensity and localization were assessed by IF of Trp53 KO<sup>Npat\_FK2AGFP</sup> AML cells treated either with NEG (left) or dTAG<sup>V</sup>-1 (right) as well as with DMSO (top), the Weel inhibitor Adavosertib (middle), or Etoposide (bottom). Hoechst (blue) served as a nuclear stain. (G) Trp53 WTNpat\_FK2AGFP and Trp53 KONpat\_FK2AGFP AML cells were treated with Adavosertib at indicated doses, with or without 50 nM dTAGV-1 treatment, and cell viability was assessed 72 hours later. Viability at each dose was normalized to the DMSO control, and dose-response curves were plotted. Each condition was assessed in triplicate. (H) Cell cycle analysis was performed using Trp53 WT<sup>Npat\_FK2AGFP</sup> and Trp53 KO<sup>Npat\_FK2AGFP</sup> AML cells following treatment with either 50 nM dTag<sup>V</sup>-1, 400 nM Adavosertib or a combination of 50 nM dTag<sup>V</sup>-1 and 400 nM Adavosertib for 24 hours. Bars indicate proportions

of cells at each cell cycle stage. Data are shown as means of three independent experiments  $\pm$  SD. P values were calculated using an unpaired t-test. (I) Proportions of apoptotic cells were assessed by Annexin V staining following either 50 nM dTag<sup>V</sup>-1, 400 nM Adavosertib or a combination of 50 nM dTag<sup>V</sup>-1 and 400 nM Adavosertib for 48 hours. P values were calculated using an unpaired t-test.

Figure 6. X	PO7 and NPAT	are predominantly	expressed in	TP53-mutated	human AN	1L
cases						

717

718

719

720

721

722

723

724

725

726

727

728

729

730

731

732

733

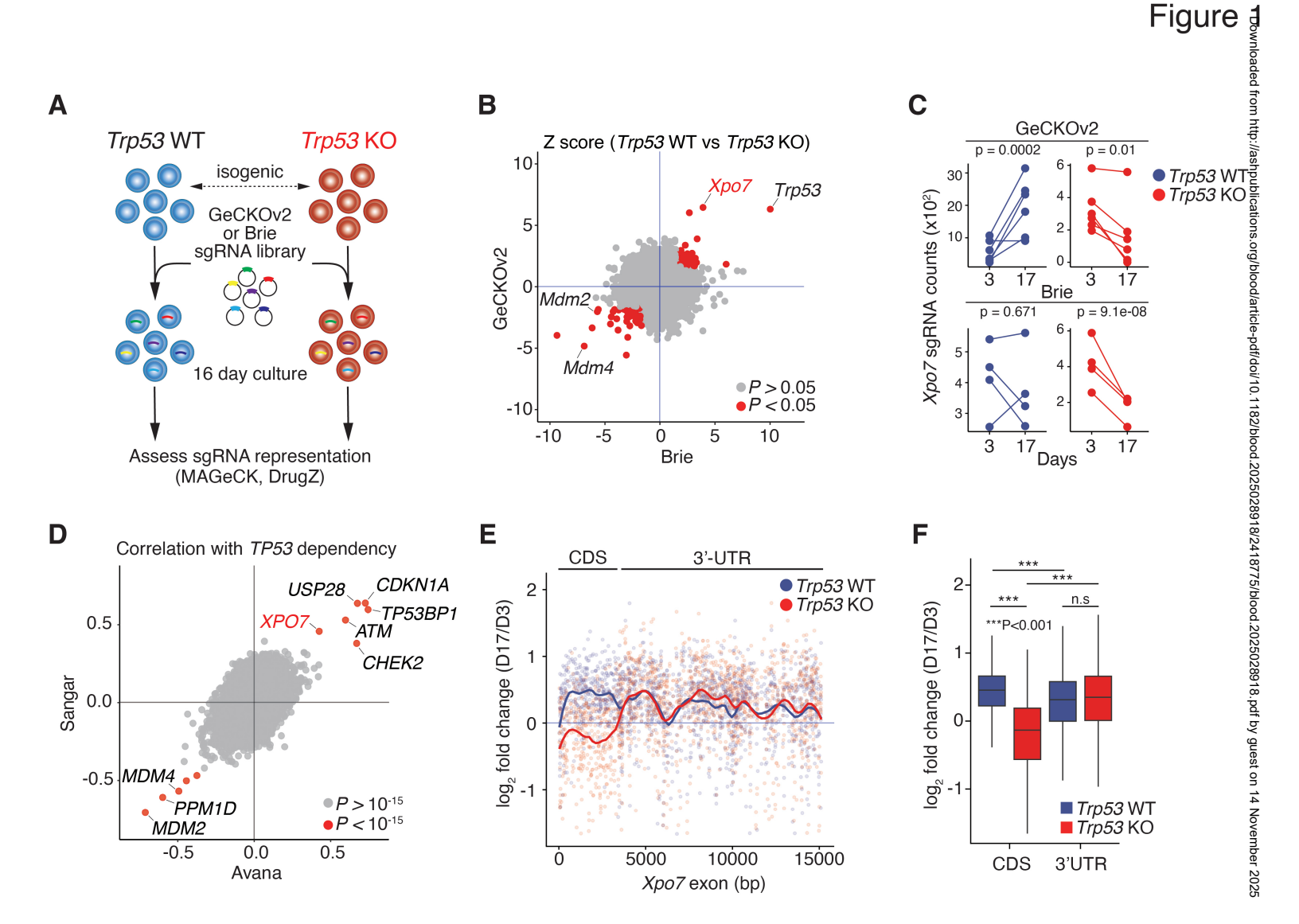
734

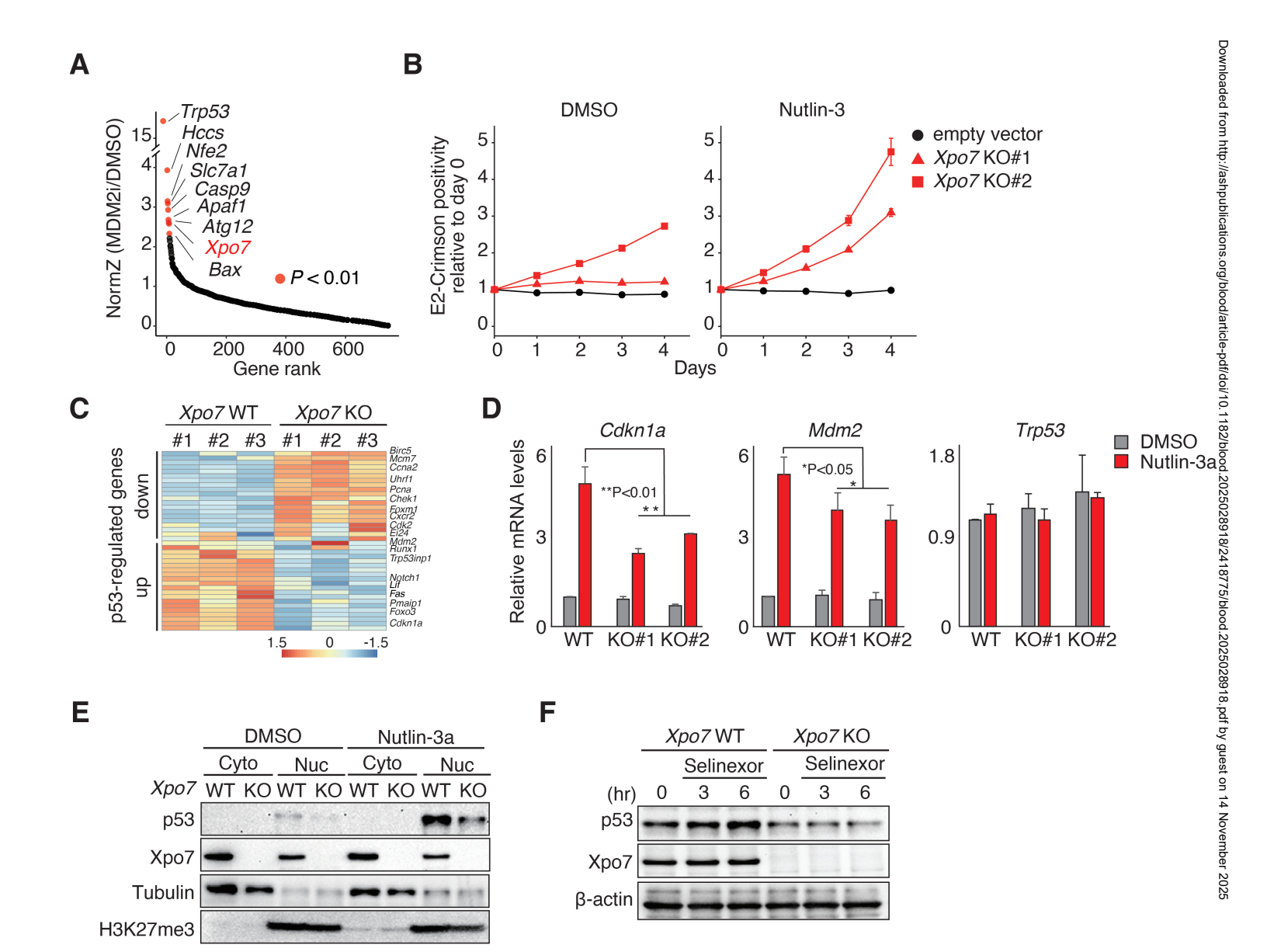
735

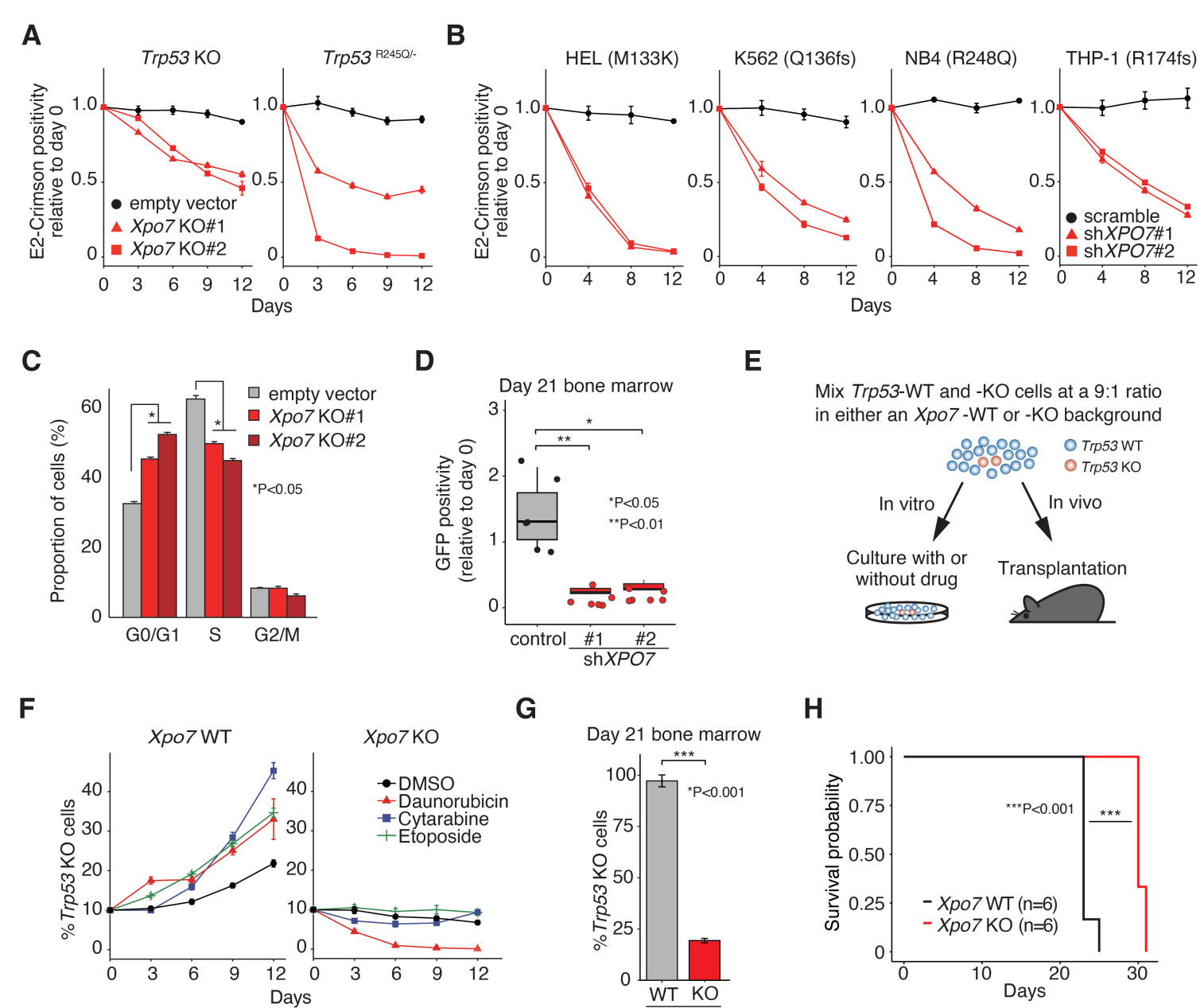
736

(A) XPO7 and NPAT mRNA levels in human AML cases, as assessed using TCGA (TP53) mutant: n=14; TP53 WT: n=148) and BeatAML (TP53 mutant: n=60; TP53 WT: n=647) cohorts. (B) NPAT and XPO7 protein levels in primary AML samples and control BM mononuclear cells (TP53 mutant: n=4; TP53 WT: n=4; control BM: n=3). (C) Schematic representation of scRNA-seq experiments using BM cells from two AML patients. (D) UMAP representation of cell type annotations for BM mononuclear cells. Cell type annotations were assigned based on transcriptomic profiles of normal BM cells<sup>48</sup> and may not reliably distinguish leukemic from non-leukemic populations in AML samples. (E) Bar graphs showing proportions of cell types in no CNA (left) and multiple CNA (right) clusters. (F) UMAP representation of XPO7 (top) and NPAT (bottom) expression in AML cells, with or without CNAs. (G) UMAP representation of estimated cell densities showing XPO7/NPAT co-expression levels (top), LSC signature score (left) and erythroid signature score (right). (H) Schematic representation of PDX AML experiments. Primary AML cells were transduced with a lentiviral vector encoding an shRNA targeting either XPO7, NPAT, or a scrambled control, along with a GFP marker, and then transplanted into immunocompromised mice. (I) Proportions of GFP-positive cells within human CD45+ cell fractions in the bone marrow (BM) were assessed by FACS 8 weeks posttransplantation. Five mice per condition were analyzed. P values were calculated using an unpaired t-test.



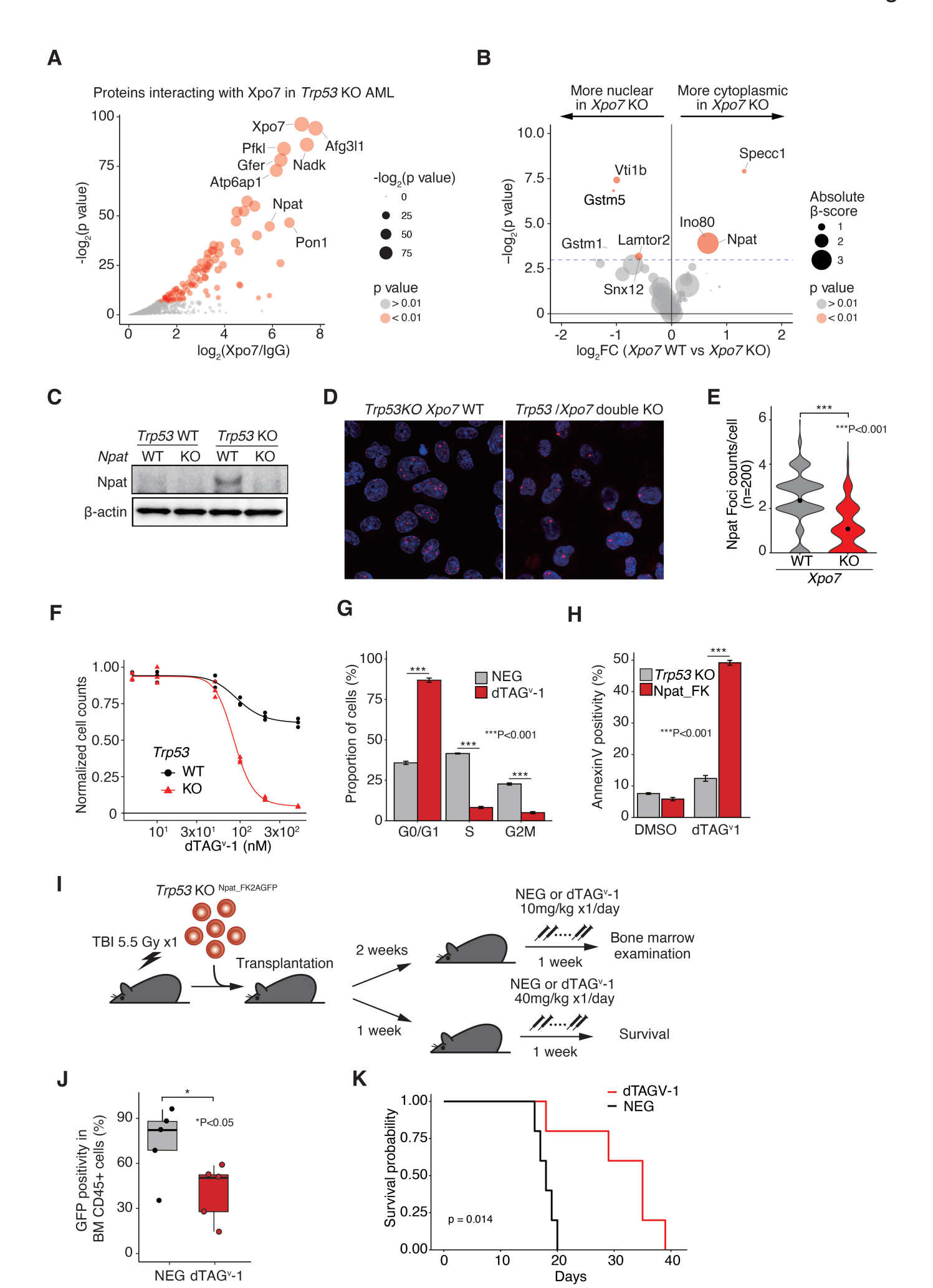


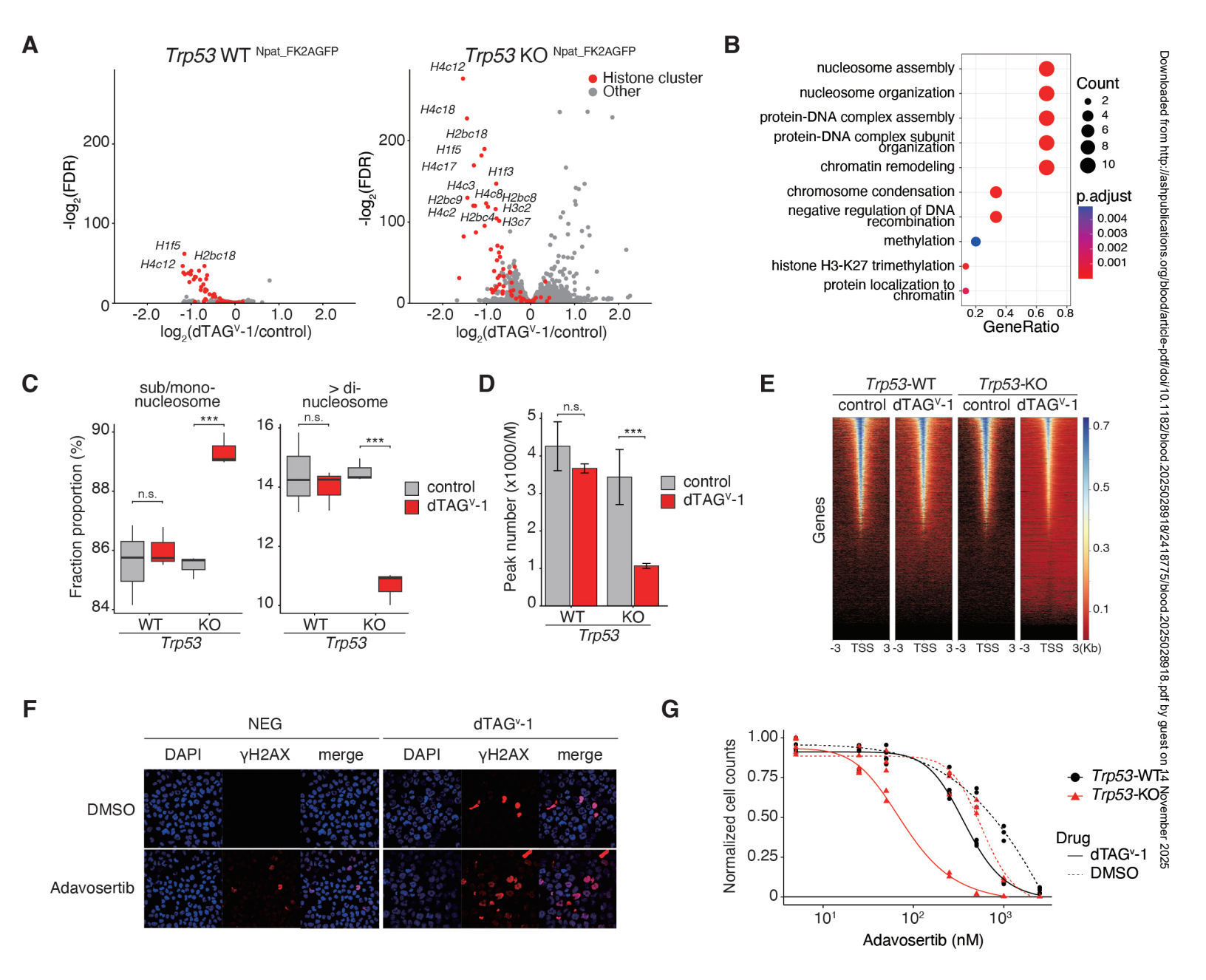


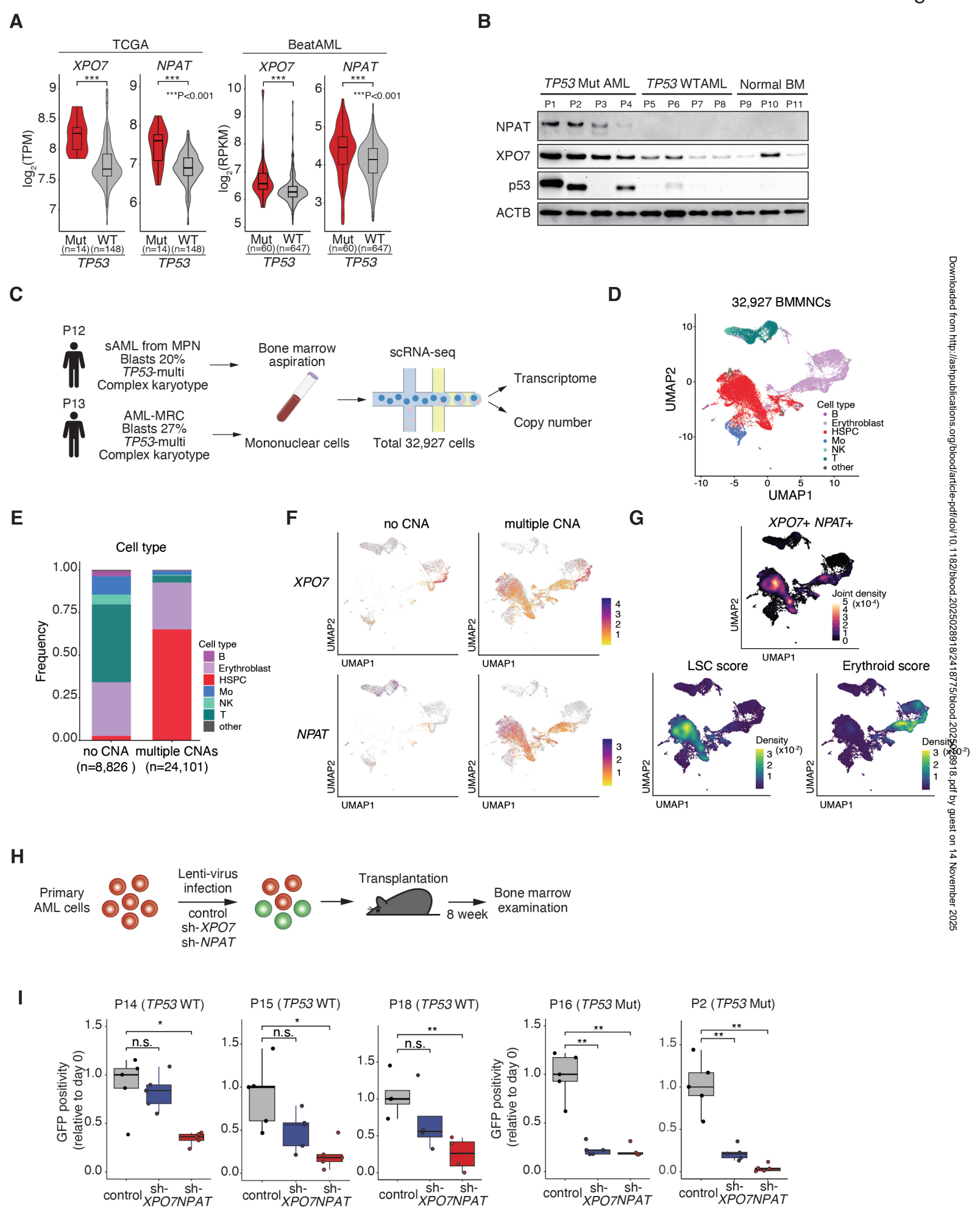


Хро7

Downloaded from http://ashpublications.org/blood/article-pdf/doi/10.1182/blood.2025028918/2418775/blood.2025028918.pdf by guest on 14 November 2025







## A Role for the XPO7-NPAT Pathway in TP53-Mutated Acute Myeloid Leukemia (AML)

#### **Context of Research**

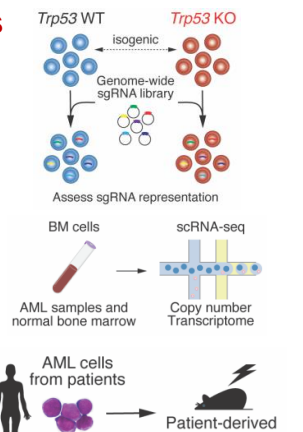
- TP53-mutated AML is refractory to standard therapies, including allogeneic HSCT.
- We performed genome-wide CRISPR-Cas9 dropout screens using isogenic Trp53-WT and -KO murine AML lines. The results were validated by human and mouse AML cell lines and primary AML samples.

#### **Material and Methods**

· CRISPR/Cas9 screen

Single-cell RNA-seq

PDX models

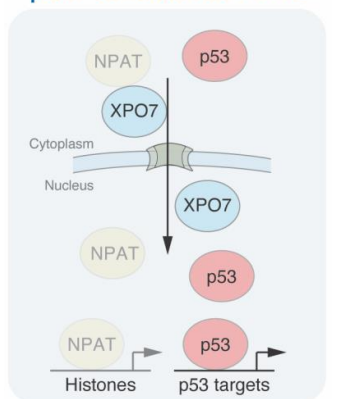


xenograft (PDX)

#### **Main Findings**

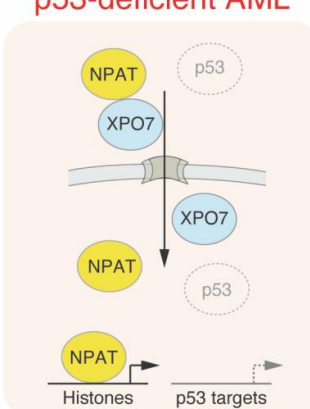
- TP53 mutation rewires the histone gene regulatory network via XPO7-NPAT pathway, creating a potential vulnerability in TP53-mutated AML cells.
- NPAT depletion compromises genomic integrity, causing replication catastrophe, particularly in p53-deficient cells.

#### p53-functional AML



NPAT levels are low. XPO7 maintains nuclear p53 levels.

#### p53-deficient AML



http://ashpublications.org/blood/article-pdf/doi/10.1182/blood.2025028918/2418775/blood.20250289 NPAT levels are high. XPO7 maintains nuclear NPAT levels.

🕓 blood

Visual Abstract

Conclusions: The findings of this study delineate key molecular mechanisms underlying TP53-mutated AML pathogenesis and identify the XPO7-NPAT axis as a critical vulnerability in this refractory leukemia subtype.

Semba et al. DOI: 10.xxxx/blood.2025xxxxxx